8. Experimental study and results

8.1. Filter determination

Early studies performed by other groups (Ward et al., 1977; Jha, 1982; Hafez and Somogyi, 1986; Ramachandran et al., 1987) were focused mainly on the determination of anti-^{220}Rn filters. These studies have shown that plastic filters such as polyethylene are very appropriate for this purpose. In contraposition, data related to filters that enhance both ^{222}Rn and ^{220}Rn diffusion are hardly available in the literature. In this section, we present the procedure followed to determine the optimum filters for detectors A and B.

The effect of a given filter is investigated by comparing the response of two identical ^{222}Rn detectors exposed at the very same ^{222}Rn concentration; one with a filter and the other without it, taken as a reference. As a ^{222}Rn detector we have used the Clipperton II probe, which has been applied by our group in soil ^{222}Rn dynamic studies (Font et al. 1999a). This probe, with a cylindrical shape of 45 cm long and 5.5 cm outer diameter, is based on a 1 cm^2 semi-conductor diode (Hamamatsu S-3590)[1] protected by special layer against friction and moisture. The upper 15 cm of the probe is a water-tight compartment that contains the electronic components, at the bottom of which the detection surface is fixed, whereas the lower part of the probe consists of a 30 cm black carbon fibre composite diffusion tube to avoid the detection of ^{220}Rn and light photons. The data processing and storing are performed by a small microprocessor and a RAM memory. A battery box providing 6 V allows the probe to operate unattended for long periods of time (Monnin and Seidel, 1998). The sampling frequency chosen has been one hour. The two probes available in our laboratory have been calibrated in our small exposure chamber.

The experimental set-up used to determine the ^{222}Rn and ^{220}Rn diffusion constant through filters is shown schematically in Figure 8.1. In this case, the pitchblende polyethylene bag is put inside the small exposure chamber; so that ^{222}Rn diffuses freely into the probe tube reaching the sensitive volume of the diode. The reference probe (that without filter) is denoted as probe 1, and the probe with the filter as probe 2. Consider the

[1]Manufactured by Hamamatsu Photonics SARL, France.

geometry sketched in Figure 8.1 with an exposure volume V_1 (cm^3) separated by the filter — of an effective surface S_2 (cm^2) — from the detection volume V_2 (cm^3) of the probe 2, the diffusion coefficient, D (cm^2 s^{-1}), at steady-state equilibrium, can be estimated from the expression given by Ward et al (1977)

$$D = \frac{\lambda \delta V_1 V_2}{S_2(V_1 + V_2)} \left[\frac{C_2}{C_1 - C_2}\right] \tag{8.1}$$

where C_1 and C_2 are the ^{222}Rn concentration measured by the probes 1 and 2, respectively. The definition of the other parameters is given in Section 5.2.2.

Table 8.1. Results of ^{222}Rn and ^{220}Rn diffusion coefficient in some filters together with the estimated delay time and the discrimination factor for the FzK diffusion chamber.

Filters	δ (cm)	D (cm^2 s^{-1})	τ_M	Discrimination factor ^{222}Rn	Discrimination factor ^{220}Rn
Polyethylene	4.5×10^{-3}	$(5.3 \pm 0.5)\times10^{-7}$	7.6 h	94.6%	0.3%
Paper (541)	0.16	$(6.1 \pm 0.7)\times10^{-4}$	14.2 min	99.8%	8.6%
Paper (542)	0.15	$(5.9 \pm 0.6)\times10^{-5}$	13.8 min	99.8%	8.8%
Glass fiber	3.5×10^{-2}	$(6.1 \pm 0.9)\times10^{-3}$	18.8 s	100.0%	81.0%

Uncertainty corresponds to one standard deviation

Filter materials tested in this experiment were commercially available polyethylene foil, two paper filters (Whatman 541 and 542)[2] and glass fiber (Glasfaser Rundfilter GF 6)[3]. Repeated measurements were performed for different thicknesses of each filter. The air was maintained at 1 atm, 24-27 ^{o}C and below 10% RH. Figure 8.2 shows the counting rate evolution of the two Clipperton probes in the case of polyethylene filter. Once the steady-state equilibrium is reached, after a time lag of approximately 10 days (Figure 8.2), the two measured the ^{222}Rn concentration during ∼20 h and the diffusion coefficient is calculated for the considered filters. The results of these mesurements are listed in Table 8.1. Also given fiven in this table are the estimated delay time, τ_M, and the discrimination factor[4] when using the FzK diffusion chamber. From all these results, we can conclude that the glass fiber and the polyethylene are the optimal filters for detectors A and B, respectively, since the former filter allows a major entry of ^{220}Rn to the sensitive volume of the FzK diffusion chamber, while the latter filter minimises the ^{220}Rn diffusion without any significant reduction of the actual indoor ^{222}Rn concentration.

[2]Manufactured by Whatman International Ltd., England

[3]The registered trade mark of Schleicher & Schuell GmbH, Germany.

[4]Calculated as the ratio $\frac{C^{ch}}{C} \simeq \frac{\tau}{\tau_M}$ (see Section 5.2.2).

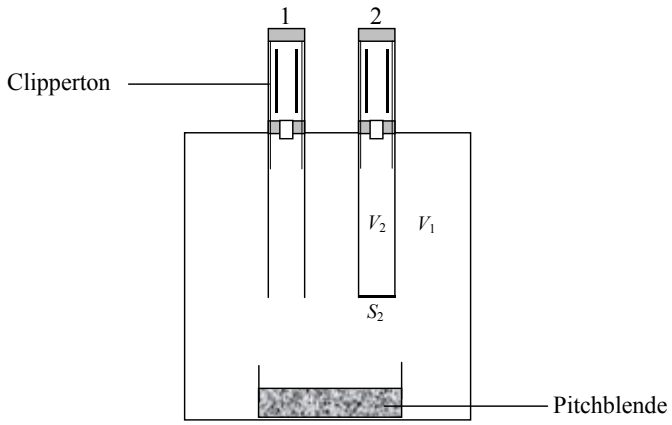

Figure 8.1. Expermiental set-up used to determine the ^{222}Rn and ^{220}Rn diffusion constants through filters.

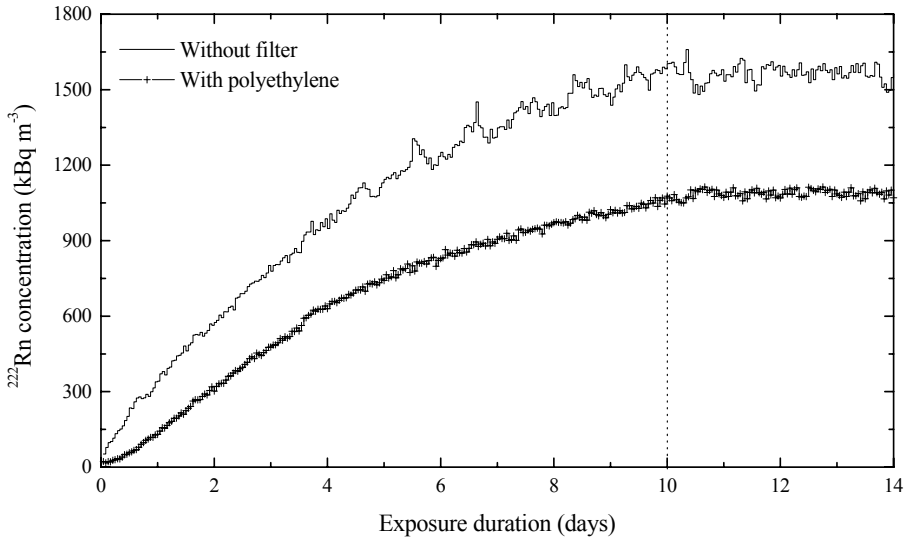

Figure 8.2. The counting rate evolution of the Clipperton probes with and without the polyethylene filter inside the small exposure chamber. The dotted line shows the time needed to reach the steady-state equilibrium.

8.2. Experimental optimisation of Makrofol response

According to Section 5.4, for simultaneous measurement of indoor ^{222}Rn and its α-emitter progeny in the presence of ^{220}Rn, the Makrofol detectors have to be etched to specific etching conditions allowing the visualisation of tracks induced by α-particles of two energy ranges: [3.0 - 5.0] MeV and [6.3 - 7.5] MeV. In this section, the optimisation of the etching conditions to achieve such α-energy windows is presented.

The required α-energy window of [3.0 - 5.0] MeV for the detectors A, B and C can be obtained by using the conventional electrochemical etching conditions previously determined in our laboratory (Baixeras et al. 1991; Font, 1993). These conditions consist of a CE for 4 h at a temperature of 40 ^{o}C, using 6 M KOH mixed with 50% ethanol[5] as etchant, followed by an ECE for 1.5 h at a frequency of 3 kHz and electric field strength of 33 kV cm^{-1}. In this work, the α-energy window of these conventional conditions have been confirmed experimentally by using both the ^{241}Am and ^{212}Bi/Po sources.

In the case of more energetic α-particles, as those registered by the detector D — i.e., between 6.3 MeV and 7.5 MeV — the etchable part of the associated tracks is located at greater depths within the detector material. Thus, the removed layer of the Makrofol detector achieved during the pre-etching process must be sufficiently high, above 43 μm according to Equation (B.2), to eliminate any track produced by α-particles with energies below 6.3 MeV; while, when finishing the ECE, the total detector thickness removed should not exceed the value of 56 μm in order not to register α-energies over 7.5 MeV. The α-energy window of the detector D could be obtained, in principle, using the same etching conditions as for the above conventional ECE simply by increasing the pre-chemical etching duration. However, because of its relatively low bulk etch rate ($\sim$4 μm h^{-1}) the duration of the pre-etching should be longer than 12 hours, which is undesirable from the practical point of view. Then, we have to find the optimum etching conditions for the detector D taking into account the compromise that the total duration of the etching process should not exceed one working journey and that the removed layer must be well-controlled during each etching step (chemical and electrochemical), since any variation of this layer may strongly affect the narrow α-energy window response of this detector. Consequently, an accurate bulk etch rate between 7 μm h^{-1} and 8 μm h^{-1} is appropriate for our purpose.

8.2.1. Bulk etch rate determination

For the determination of the suitable bulk etch rate for the detector D, we have varied the etching temperature, the KOH molarity and the percentage of ethanol mixture

[5]The alcohol purity used in this study is 96 %.

of the etchant (M, %). For each chemical etching condition, 10 Makrofol square plates, with an approximate dimension of 2×2 cm^2 and 500 μm thick, were chemically etched for five hours. The removed layer of each plate was measured as a mean thickness difference before and after the etching using an electronic inductive trigger (MILITRON FEINPRÜF)[6] with an accuracy of $\pm$ 1 μm.

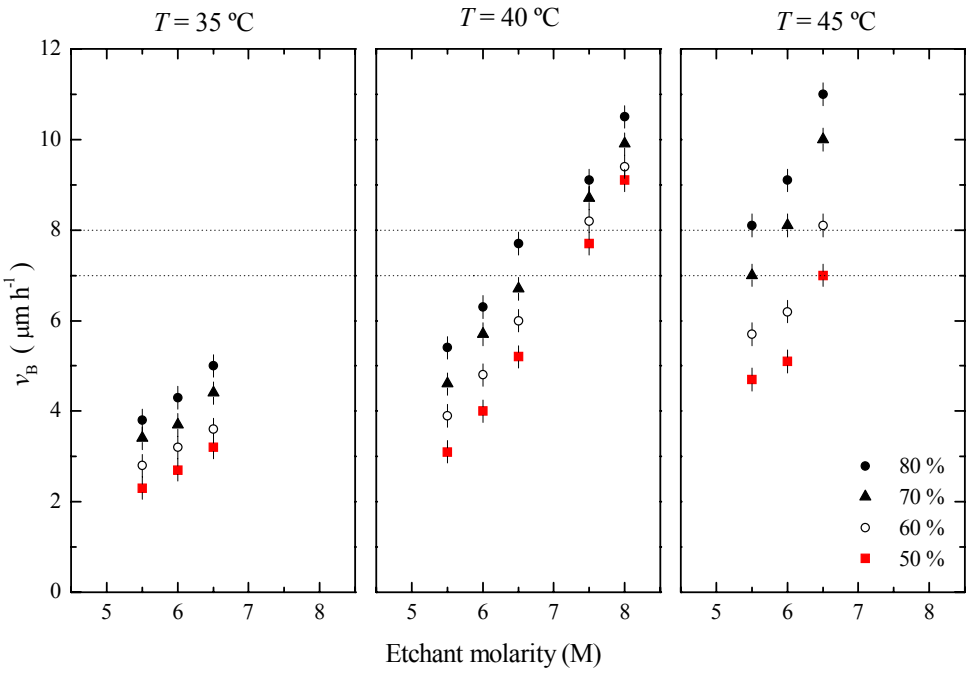

Figure 8.3. Bulk etch rate (v_B) as a function of the etchant molarity at different values of % ethanol and etching temperature. The horizontal dotted lines indicate the interval of the required optimum bulk etch rates (between 7 μm h^{-1} and 8 μm h^{-1}).

The results of this study are presented in Figure 8.3. The uncertainties found are due mainly to the intrinsic scattering of the detector thickness. It is shown in this figure that the bulk etch rate increases when increasing the etching temperature, the KOH molarity or the percentage of ethanol mixture in the etchant. The required bulk etch rate, between 7 μm h^{-1} and 8 μm h^{-1}, can be obtained using any concentration of the etchant between (6.5 M, 80 %) and (7.5 M, 50%) at an etching temperature of 40 ^{o}C or between (5 M, 80 %) and (7 M, 50 %) at 45 ^{o}C. Taking into account the alcohol evaporation when increasing

[6]Manufactured by Militron High Technology Ltd., Germany.

the etching temperature and/or the ethanol quantity, especially for long CE duration, a dissolution of 7.5 M KOH mixed with 50 % ethanol at an etching temperature of 40 ^{o}C has been chosen to be the appropriate CE conditions for the detector D. Given these CE conditions, we have plotted in Figure 8.4 the removed layer obtained varying only the CE duration, t_{CE}. According to this figure, the removed layer has a lineal behaviour with respect to the CE duration showing no reduction in the chemical activity of the etchant at least up to 7 h. The bulk etch rate obtained by regression line of the experimental data is

$$v_{\mathrm{B}} = (7.8 \pm 0.1)\ \mu\mathrm{m\ h}^{-1}\ (\mathrm{R}^2 = 0.988) \tag{8.2}$$

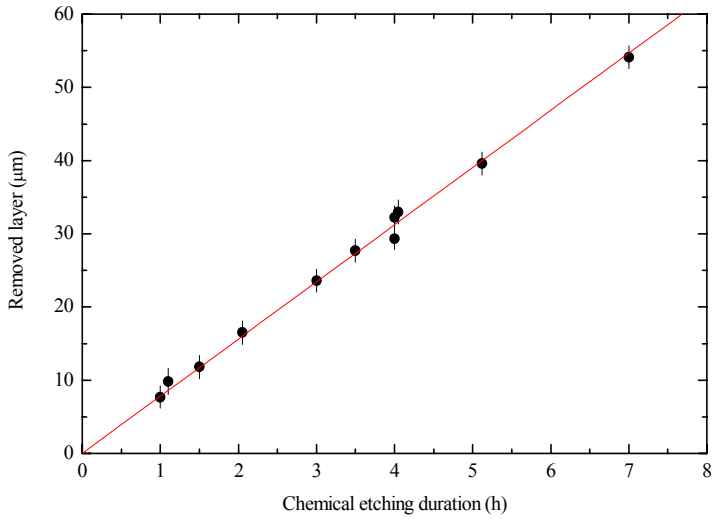

Figure 8.4. The removed layer as a function of the chemical etching duration, t_{CE}, using as etchant a solution 7.5 M KOH mixed with 50 % ethanol and an etching temperature of 40 ^{o}C. The solid line is a least-square adjustment of the data.

8.2.2. CE time determination

Once the optimum bulk etch rate is found for the detector D in the previous section, it is of importance now to determine the required pre-etching duration to obtain the energy window of interest. In this context, the response of Makrofol detectors was investigated as a function of incident α-energies. For this purpose, 7 sets of Makrofol detectors, covered with aluminised Mylar of 3 μm thick, were irradiated to α-particles with energies ranging from 2.0 MeV to 8.0 MeV (using the ^{241}Am and ^{212}Bi/Po sources of the Section 7.4) and

were electrochemically etched at the optimum chemical conditions by varying only the pre-etching time from 0 h to 6 h. The other parameters, which correspond to the ECE, were fixed unvaried at one hour of duration with an electric field strength 33 kV cm^{-1} and a frequency of 3 kHz.

The detector efficiencies for the considered α-energy are calculated as the ratio of the track density to the expected fluency estimated from the SBD reference measurements. Figure 8.5 shows the Makrofol detector efficiency as a function of the α-energy for various pre-etching times. We observe a shift of the Makrofol α-energy window response in the direction of high energies when increasing the pre-etching time. The decrease in the energy window width, from ~1.5 MeV at low α-energies to ~0.8 MeV at high α-energies, is due mainly to the no lineal range-energy dependence of α-particles within the Makrofol detector as predicted by the Srim-2000 code (see Appendix B). No changes in the background track densities were observed for these ECE conditions when varying the pre-etching time, resulting in a mean value of about (11 ± 4) cm^{-2}.

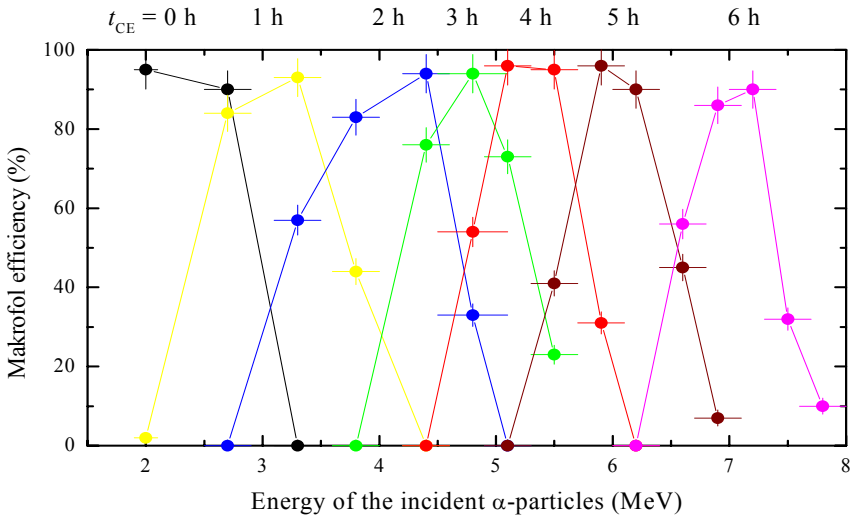

Figure 8.5. Electrochemical etched Makrofol efficiency as a function of the energy of the incident α-particles at different pre-etching times. The CE and ECE conditions are given in the text.

From each of the α-energy response obtained in the previous figure, the corresponding values of its lower and upper α-energy threshold (E_{min} and E_{max}, respectively) were taken. By plotting these values in Figure 8.6 as a function of the pre-etching time,

a quite lineal time-dependence is observed for $E_{\min}$ and $E_{\max}$. This behaviour leads to determine empirically the removed layer we must achieve in a CE of the Makrofol detector to obtain the required α-energy window of [6.3 - 7.5] MeV. According to the fitted values obtained, the pre-etching time necessary to obtain this α-energy window response is 6 hours. Finally, the optimum ECE conditions found for the detector D are:

Etchant	:	KOH **7.5** M mixed with 50% ethanol
Temperature	:	40 ^{o}C
Pre-etching duration	:	**6** h
Frequency	:	3 kHz
Electric field strength	:	33 kV cm^{-1}
ECE duration	:	**1** h

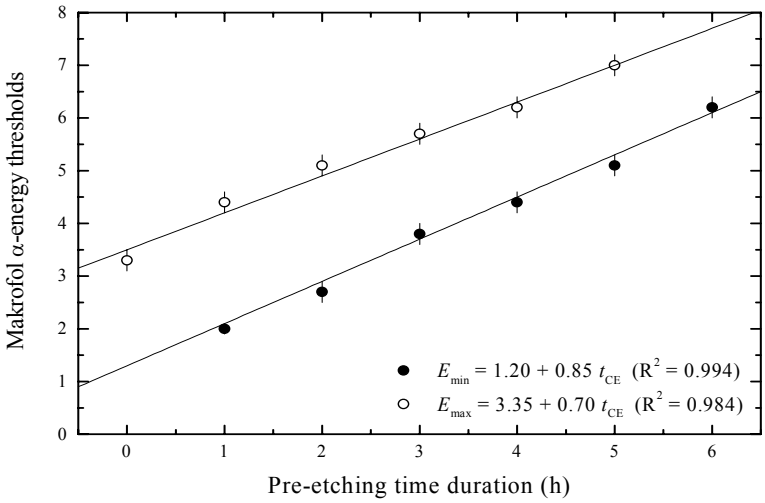

Figure 8.6. The low and upper energy thresholds of electrochemical etched Makrofol detectors as a function of the pre-etching time. The CE and ECE conditions are given in the text.

8.3. Experimental calibration

Since only ^{222}Rn gas offers the possibility to be isolated for individual irradiation, the experimental calibration of the passive integrating system developed in this study is performed firstly in pure ^{222}Rn atmospheres.

8.3.1. Detector A calibration in front of ^{222}Rn

As a consequence of the participations of our group in several international intercomparisons organised by the National Radiological Protection Board (NRPB, England) during the 90's decade as well as in joint collaborations with the Department of Physics and Materials Science (DPMS) of Hong Kong University and the National Institute of Radiological Sciences (NIRS, Japan), a series of calibration exercises were conducted during the period 1997 - 2001. In these calibration exercises, about 16 sets of 10 identical Makrofol detectors each one, enclosed within a FzK diffusion chamber using a fiber glass filter (detector A), have been irradiated under different ^{222}Rn exposures. A description of the characteristics of these exposure facilities as well as the relation of sets and measurement techniques used appear in Table 8.2. During transport and storage, all the detectors were heat-sealed in radon-proof bags to minimise unwanted exposures. Once irradiated, the detectors were returned to our laboratory to be etched under the conventional etching conditions. The net track density values obtained, after background subtraction, as a function of the associated ^{222}Rn exposures are presented in Figure 8.7. According to this figure, the net track density of the detector A shows saturation at ^{222}Rn exposures above 1500 kBq m^{-3} h. Below this value, the detector response is lineal and the sensitivity obtained — using a least-square fitting curve — is (0.76 ± 0.02) cm^{-2} kBq^{-1} m^3 h^{-1} (R^2 = 0.982), which is very close to that estimated by the Monte-Carlo simulation.

Table 8.2. Characteristics of the exposure facilities as well as the relation of sets and measurement techniques used to calibrate the detector A against ^{222}Rn.

Centre	Exposure facility	Measurements	Year	Sampling technique
NRPB	43 m^3 walk-in ^{222}Rn chamber	3	1997	Ionisation chamber
		3	1998	
		3	1999	
		3	2000	
DPMS	410 L ^{222}Rn/^{220}Rn small chamber	3	2001	Scintillation cell
NIRS	150 L ^{222}Rn/^{220}Rn small chamber	1	2001	Scintillation cell

The long period of the above irradiations (in terms of years) makes evidence of the consistency and the reproducibility of the detector A response against ^{222}Rn exposure. The saturation effect found for high ^{222}Rn levels (above 1500 kBq m^{-3} h) is not only a limitation of the semi-automatic system due to the track overlapping effect, but it is also an intrinsic property of the electrochemically etched Makrofol detectors. At high exposure values, appreciable amounts of the incident α-particles are simply not recorded. This issue was verified by re-counting manually the track saturated detectors using the microfiche reader of the Section 7.2. However, the saturation effect does not suppose an obstacle since, in a preliminary survey carried out by our group in the Barcelona area using similar detectors, the typical values of track densities found for 3 - 4 month exposure were mostly below 400 cm^{-2} (Amgarou et al., 2001a). It is to remark that until 2000, we have used Makrofol detectors with a thickness of 300 μm, instead of the 500 μm thick chosen recently. As shown in Figure 8.7, by maintaining the same electrochemical etching conditions, especially the electric field strength, the response of the Makrofol detector is not affected by the thickness chosen for this last. To keep the same electric field strength of 33 kV cm^{-1}, we have to apply an AC effective voltage of ∼1.6 kV for a detector thickness of 500 μm and of ∼1 kV for a detector thickness of 300 μm.

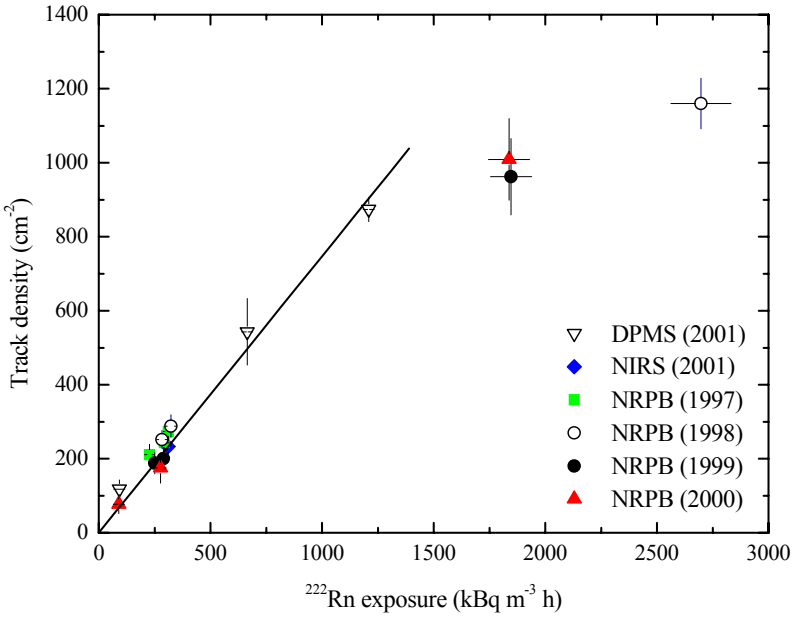

Figure 8.7. Calibration curve for the detector A against pure ^{222}Rn atmospheres.

8.3.2. Detector B calibration in front of ^{222}Rn

In the case of detector B, its experimental calibration with pure ^{222}Rn atmospheres was carried out in the DPMS and the NIRS centres to where 3 sets and one set (of 10 detectors esch set), respectively, were sent to be irradiated together with the detectors A. Figure 8.8 shows the net track densities obtained for these detectors as a function of the associated ^{222}Rn exposures. We observe a lineal behaviour of the detector B response within the ^{222}Rn exposure interval between 0 and 1500 kBq m^{-3} h. Its sensitivity obtained by a lineal regression curve, (0.76 ± 0.02) cm^{-2} kBq^{-1} m^3 h^{-1} (R^2 = 0.998), is identical to that found for the detector A. This finding is not surprising since the difference between the ^{222}Rn discrimination factors of the glass fiber and polyethylene filters, chosen respectively for the detectors A and B, can be considered as negligible taking into account the associated uncertainties (see Table 8.1).

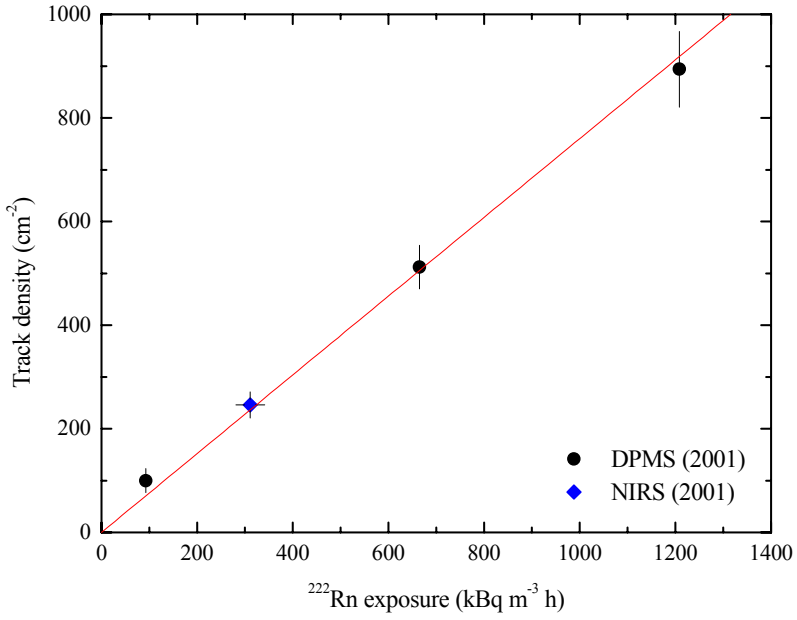

Figure 8.8. Calibration curve for the detector B against pure ^{222}Rn atmospheres.

In all the above experiments, the transit control was ensured by keeping additional detectors unirradiated and tightly stored during the manipulation, irradiation and transport. No changes in the transit track densities were observed for the detector A and B.

Their mean value obtained, (8 ± 3) cm^{-2}, is very comparable to that of the detector D. Thus, all the detectors used in this study (A, B, C and D) are expected to have the same background level of about (10 ± 3) cm^{-2}.

We can conclude that the agreement found between the SIMAR computer code prediction and the experimental calibration of the detectors A and B with pure ^{222}Rn atmospheres is satisfactory. Hence, we assume that the theoretical sensitivity values calculated for the detector A, C and D with respect to ^{222}Rn daughters and ^{220}Rn are correct. Using these values, the final equations giving the track densities of the detectors A, B, C and D in front of ^{222}Rn, ^{220}Rn, ^{218}Po and ^{214}Po exposures are

$$\rho_{\mathrm{A}} = 0.76\chi_{^{222}\mathrm{Rn}} + 0.12\chi_{^{220}\mathrm{Rn}} \tag{8.3}$$

$$\rho_{\mathrm{B}} = 0.76\chi_{^{222}\mathrm{Rn}} \tag{8.4}$$

$$\rho_{\mathrm{C}} = 0.74\chi_{^{222}\mathrm{Rn}} + 0.71\chi_{^{218}\mathrm{Po}} + 0.66\chi_{^{214}\mathrm{Po}} + 1.37\chi_{^{220}\mathrm{Rn}} \tag{8.5}$$

$$\rho_{\mathrm{D}} = 0.66\chi_{^{214}\mathrm{Po}} + 0.26\chi_{^{220}\mathrm{Rn}} \tag{8.6}$$

where $\chi_{^{222}\mathrm{Rn}}$, $\chi_{^{220}\mathrm{Rn}}$, $\chi_{^{218}\mathrm{Po}}$ and $\chi_{^{214}\mathrm{Po}}$ are respectively the ^{222}Rn, ^{220}Rn, ^{218}Po and ^{214}Po exposures, in units of kBq m^{-3} h, defined as the time-integrated of their associated concentrations during the exposure period.

8.4. Uncertainty measurements

Taking into account the substraction of the background track density and the optical counting field used by the semi-automatic system, the Relative Standard Deviation (RSD) of the radiation-induced track density, $\rho_{\mathrm{net}} = \rho - \rho_{\mathrm{bg}}$, from a single measurement of any of the detectors A, B, C and D is given by

$$\mathrm{RSD}(\rho_{\mathrm{net}}) = \frac{\sqrt{\sigma^2 + \sigma_{\mathrm{bg}}^2}}{\rho_{\mathrm{net}}} = \frac{\sqrt{\sigma^2 + \sigma_{\mathrm{bg}}^2}}{\rho - \rho_{\mathrm{bg}}} \tag{8.7}$$

where ρ and ρ_{bg} are respectively the gross and background track densities whose standard deviations are σ and σ_{bg}. These last are assumed to be of statistical origin following a Poisson distribution (i.e., having variances equal to their expected values). In general, systematic uncertainties may also have a large effect on the measurement, but this category of uncertainty might not be accepted as inevitable limitation of the detector and should be identified and minimised. On the other hand, the standard deviation of the gross track density, which is defined as the ratio between the number of tracks (n) and the optical counting field (F), can be calculated as

$$\sigma = \sqrt{\frac{\mathrm{n}}{\mathrm{F}^2} + \left[\frac{\mathrm{n}}{\mathrm{F}}\ \mathrm{RSD(F)}\right]^2} \tag{8.8}$$

where RSD(F) is the relative uncertainty of the semi-automatic optical field, which was estimated to be 2% using a grid scale of 1/100 cm precision. By replacing $\rho = \frac{\mathrm{n}}{\mathrm{F}}$ in Equation (8.8), Equation (8.7) becomes

$$\mathrm{RSD}(\rho_{\mathrm{net}}) = \frac{\sqrt{\left[\frac{\rho}{\mathrm{F}} + (0.02\rho)^2\right] + \sigma_{\mathrm{bg}}^2}}{\rho - \rho_{\mathrm{bg}}} \tag{8.9}$$

Figure 8.9 shows the relative standard deviation of the detectors A, B, C and D as a function of the net track density ρ_{net}. According to this figure, the relative standard deviation decreases with increasing the net track density and reaches a value of 5% at saturation levels. At low track density (below 100 cm^{-2}), the relative standard deviation is above 15%. To prevent high statistical uncertainties ($> 40\%$), the radiation induced track density should be above the value of 20 cm^{-2}.

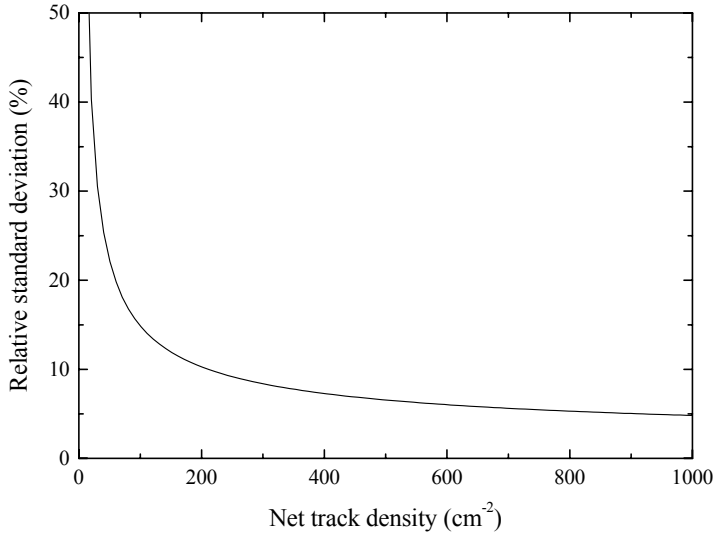

Figure 8.9. The relative standard deviation of the detectors A, B, C and D as a function of the net track density.

8.5. Limits of detection and quantification

The limits of detection are one of the most important performance characteristics of any measurement process and are based entirely on the error-structure of this. According to Currie (1968), three different limits of detection have to be considered: the critical level, the detection limit and the quantification limit.

8.5.1. Critical level:

The critical level is the minimum significant value, estimated with a specified confidence level, above which an outcome or observed instrument response or signal may indicate the presence of a net activity or concentration of the radionuclide subject to measurement. At the 95% confidence level, this magnitude in terms of track density units is expressed as

$$L_{\mathrm{C}}\ (\mathrm{cm}^{-2}) = 1.645\sigma_0 \tag{8.10}$$

where σ_0 is the standard deviation of the net track density under the null hypothesis (the true value is equal to zero).

The critical level is result-specific and is intended to be used a posteriori (i.e., after the measurement is conducted) to test the experimental result obtained.

8.5.2. Detection limit:

The detection limit is the smallest net activity or concentration of the radionuclide subject to measurement that can be detected with a given confidence level (usually 95%) and is defined, in terms of track density units, as

$$L_{\mathrm{D}}\ (\mathrm{cm}^{-2}) = 2.71 + 3.29\sigma_0 \tag{8.11}$$

The detection limit is an inherent property of the measurement process whose determination should be done a priori (i.e., before the measurement is conducted).

8.5.3. Quantification limit:

The quantification limit is the signal level at which any measurement can be performed with a maximum tolerable statistical uncertainty and it can simply be written, in terms of track density units, by

$$L_{\mathrm{Q}}\ (\mathrm{cm}^{-2}) = k_{\mathrm{Q}}\sigma_{\mathrm{Q}} \tag{8.12}$$

where k_Q is the inverse of the desired relative standard deviation and σ_Q is the standard deviation observed for track densities at the limit L_Q.

The quantification limit defines the precision of the measurement and, similarly to the detection limit, its determination should be done prior to sample analysis. As shown in Figure 8.9, the minimum net track density necessary to obtain a precision of 10% with our detection system is 200 cm^{-2}.

The a priori determination of the detection limit is possible only in the case of ^{222}Rn measurement by means of the detector B, since this last has the unique influence of the background track density. Thus, the variance of the net track densities, σ_0^2, of this detector when the observed counts are near-background levels ($\rho_B - \rho_{bg} \simeq 0$) can be estimated as

$$\sigma_0^2 \simeq \sigma_{bg}^2 + \sigma_{bg}^2 \simeq 2\sigma_{bg}^2 \tag{8.13}$$

Taking into account the exposure time, t_e (h), the detection limit in terms of ^{222}Rn concentration units is given by

$$L_D \text{ (Bq m}^{-3}) = \frac{2.71 + 4.65\sigma_{bg}}{0.76 t_e} \tag{8.14}$$

being 0.76 the detector B sensitivity in front of ^{222}Rn. Using the value of the background track density found in the Section 8.3.2, the minimum detectable concentration of ^{222}Rn is 10 Bq m^{-3} for an eventual exposure time of 90 days. It is of great interest to point out that at low ^{222}Rn levels, the exposure time should be increased in order to diminish its minimum detectable concentration. Nonetheless, at high ^{222}Rn levels, the exposure time must be reduced in order to avoid the detector saturation effect even if it supposes an increase of the associated detection limit, since this last will be smaller than the actual concentration to be measured.

When the airborne ^{220}Rn, ^{218}Po and ^{214}Po concentrations are measured using the detectors A, C and D, the response of these last are not only influenced by the background track density but also by the presence of the other radionuclides (e.g., ^{222}Rn in the case of detector A, ^{222}Rn+^{220}Rn+^{214}Po in the case of detector C, and ^{220}Rn in the case of detector D). We say, therefore, that track density interferences may occur as a result of the α-emissions from the airborne ^{222}Rn, ^{220}Rn, ^{218}Po and ^{214}Po. The level of these interfering radionuclides can be considered part of the detector background. Consequently, it is not possible to determine a priori the ^{220}Rn, ^{218}Po and ^{214}Po minimum detectable concentration. However, qualitative decision concerning the presence of ^{220}Rn is necessary because any measurable concentration of this gas affects strongly the results of airborne ^{218}Po and ^{214}Po concentrations.

In order to attribute the reading difference between the detectors A and B to ^{220}Rn exposure, especially when the track density of the detector A is of the same order than that of the detector B, one must invoke an appropriate statistical criterion. This last is largely satisfied by using the ^{220}Rn critical level, which should be calculated from the standard deviation of track densities observed for the detector B (σ_B) as

$$L_C(^{220}\text{Rn}) = 1.645\sigma_0 \simeq 2.33\sigma_B \tag{8.15}$$

being $\sigma_0 \simeq \sqrt{2}\sigma_B$. Then, as stated by Currie (1968), if $\rho_A - \rho_B \leq L_C$, the decision *not detected* should be reported and an upper limit of ^{220}Rn exposure should be given as $\frac{2.33\sigma_B}{0.12}$ (where 0.12 corresponds to the detector A sensitivity in front ^{220}Rn); while, if $\rho_A - \rho_B \geq L_C$, the decision *detected* should be reported and the estimated value of ^{220}Rn concentration with the associated uncertainty should be given.

Table 8.3. Results of simultaneous irradiation of the detectors A and B to ^{222}Rn and ^{220}Rn under different values of their exposures.

	References measurements (kBq m^{-3} h)		Our passive integrating system Track density (cm^{-2})			(kBq m^{-3} h)	
Centre	^{222}Rn	^{220}Rn	ρ_A	ρ_B	L_C	^{222}Rn	^{220}Rn
DPMS	99 ± 1	70 ± 2	102 ± 21	90 ± 20	47	118 ± 26	<390
	633 ± 4	522 ± 4	558 ± 37	549 ± 26	61	722 ± 34	<510
	991 ± 3	647 ± 5	681 ± 49	676 ± 47	110	889 ± 62	<920
NIRS	109 ± 11	1250 ± 250	235 ± 35	93 ± 21	49	122 ± 27	1180 ± 350

To verify the usefulness of this statistical criterion, three sets and one set, respectively, of 10 dosimeters were irradiated simultaneously to ^{222}Rn and ^{220}Rn at the DPMS and NIRS centres under different values of their exposures. The comparison between the results obtained by our system and those given by the centres are summarised in Table 8.3. It can be seen in this table that the ^{220}Rn critical level is a good criterion for testing its presence by means of the detectors A and B. In those sites with similar levels of ^{222}Rn and ^{220}Rn, the determination of the actual concentration of this last is not possible and only an upper limit could be estimated. This is due to the fact that the sensitivity of the detector A with respect to ^{220}Rn is lower than that of ^{222}Rn. In contraposition, one of the main advantages of our system with respect to other passive methods aimed to measure the airborne ^{222}Rn progeny, is that our system takes into account the ^{220}Rn contribution to the detector readings and lets the additional estimation of its concentration at high levels when compared with ^{222}Rn.

8.6. Equilibrium factor determination

The performance of the method developed in this study with active detectors was tested at the NRPB centre, in which 3 sets (each one with 5 of our dosimeters) were irradiated under different ^{222}Rn exposures but at varied equilibrium factors. This facility is the European regional reference laboratory for ^{222}Rn and its progeny measurement, calibration and intercomparison purposes. The ^{222}Rn levels to which the dosimeters were exposed ranged from 90 kBq m^{-3} h for the exposure 1 to ∼2000 kBq m^{-3} h for exposure 3. The equilibrium factor is controlled by means of an aerosol generator that reduces the plate-out effect of the decay products and an electrostatic precipitator with a fan for their subsequent collection. The ^{222}Rn daughters are continuously monitored using the wire-screen technique together with a back-up filter (Cliff, 1990).

Table 8.4 summarises the averaged values of ^{222}Rn progeny equilibrium factor as obtained with our passive integrating system and by the NRPB active monitors. The equilibrium factor values of our detection system agree with those given by the NRPB, taking into account the associated uncertainties. The overestimation given by our system at low equilibrium factor, where the plate-out effect is very important, is due mainly to the detector D. This may suggest that this detector has probably recorded a fraction of the ^{214}Po deposited directly on its surface. In the third exposure, the levels of ^{222}Rn and its decay products were extremely high (above 1500 kBq m^{-3} h); so that, the detectors used have suffered from the problem of the track saturation effect. Because of the large overall uncertainties on the equilibrium factor, further investigations of the parameters affecting the measurement process are required to improve the system precision and to optimise its response under different exposure conditions.

Table 8.4. The comparison between the values of ^{222}Rn progeny equilibrium factor obtained by our passive integrating system and those given by the NRPB active monitor.

	Equilibrium factor	
	This work	NRPB
Exposure 1	0.48 ± 0.15	0.38 ± 0.03
Exposure 2	0.37 ± 0.11	0.22 ± 0.04
Exposure 3	0.61 ± 0.18	0.84 ± 0.08

8.7. Application indoors

A field test of our passive integrating system was carried out in an inhabited Swedish single-family house as a result of a collaboration with the Lund University. The reason for choosing a house in the North of Europe comes because of the high values of the ^{222}Rn concentration found previously in this region within the frame of an European Union project in which a coordinated survey of the Lund-Kiel-Leipzig-Montpellier-Barcelona-Rome areas was carried out (Font et al., 1999b). This house has two well-differentiated parts: the main building and the annexes. The first one is the major part of the house, where the most used rooms are placed and has a crawl-space of about one meter depth. The annexes are in direct contact with soil and include a guest room, a storage zone and the garage. Except the crawl-space, which is naturally-ventilated, the house is isolated from exterior with all the windows and the doors closed. Two sets of 5 dosimeters were exposed for one month (18 September - 19 October 2001) in the crawl-space and in the guest room.

Table 8.5. Results from indoor exposure of our passive integrating system in a Swedish house.

	Crawl-space	Guest room
^{220}Rn (Bq m^{-3})	<270	<440
^{222}Rn (Bq m^{-3})	288 ± 18	263 ± 30
^{218}Po (Bq m^{-3})	120 ± 100	170 ± 110
^{214}Po (Bq m^{-3})	36 ± 28	63 ± 31
F	0.18 ± 0.12	0.33 ± 0.15

The ^{222}Rn, ^{220}Rn, ^{218}Po and ^{214}Po concentrations measured by our dosimeter as well as the estimated equilibrium factors for the crawl-space and the guest room are given in Table 8.5. The low equilibrium factor value obtained in the crawl-space could be attributed mainly to ventilation. The ^{222}Rn concentration found is within the range measured previously (Font et al., 1999b). In the case of the guest-room, the annual effective dose, which was estimated using the conversion factor of 1.1 Sv J^{-1} m^3 h^{-1} and a permanency time of 7000 h per year suggested in Section 2.3 for indoor exposure to ^{222}Rn progeny in private homes, is equal to (3.7 ± 1.8) mSv y^{-1}. This result suggests the usefulness of our system to carry out routine surveys for ^{222}Rn level measurements in private homes and in workplaces in order to estimate the associated annual effective dose received by the general public and the workers.